

Mounting Parameter Estimation From Velocity Vector Observations for Land Vehicle Navigation

Quan Zhang , Yuanqian Hu, Shanshan Li, Tisheng Zhang, and Xiaoji Niu 

Abstract—A velocity model composing speed sensors and motion constraints is used as the direct and effective auxiliary information of global navigation satellite system (GNSS)/inertial navigation system integrated systems to improve the land vehicle navigation accuracy under interfered or blocked GNSS signal environments. The precise determination of the mounting parameter (the geometric relationship between sensors), including mounting angle and lever arm, is necessary to realize the full potential of velocity assistance. In this article, we propose an optimal mounting parameter estimation scheme based on the velocity vector observations. The quaternion-based optimal attitude determination method is used to estimate the mounting angle, and the weighted recursive least squares are applied to estimate the lever arm. A land vehicle test and an agricultural tractor test are carried out to verify the feasibility and correctness, and inertial measurement units (IMUs) of different grades, especially the micro electro mechanical system (MEMS) IMUs, are used. The results show that the attitude errors, especially the heading error, are the main factors influencing mounting angle estimation and that the statistical lateral velocity based on the estimated mounting parameters is better than 0.03 m/s, thus better satisfying vehicle motion constraints.

Index Terms—Attitude determination, land vehicle navigation, MEMS inertial measurement unit (IMU), mounting angle, velocity model.

I. INTRODUCTION

THE integration of the global navigation satellite system (GNSS) and inertial navigation system (INS) can provide high-precision (e.g., centimeter level) positioning navigation solutions for land vehicles [1]. However, the major drawback of the GNSS is the accuracy degradation due to poor satellite

Manuscript received July 4, 2020; revised December 10, 2020 and March 19, 2021; accepted April 12, 2021. Date of publication May 3, 2021; date of current version December 20, 2021. This work was supported in part by the National Natural Science Foundation of China under Grant 41604020 and in part by the Fundamental Research Funds for the Central Universities under Grant 2042019kf0219 (Corresponding author: Xiaoji Niu.)

Quan Zhang, Tisheng Zhang, and Xiaoji Niu are with the GNSS Research Center, Wuhan University, Wuhan 430079, China, and also with the Collaborative Innovation Center of Geospatial Technology, Wuhan University, Wuhan 430079, China (e-mail: zhangquan@whu.edu.cn; zts@whu.edu.cn; xjniu@whu.edu.cn).

Yuanqian Hu and Shanshan Li are with the Qianxun Spatial Intelligence, Inc., Shanghai 200438, China (e-mail: yuanqianhu@whu.edu.cn; shanshanli@whu.edu.cn).

Color versions of one or more figures in this article are available at <https://doi.org/10.1109/TIE.2021.3075883>.

Digital Object Identifier 10.1109/TIE.2021.3075883

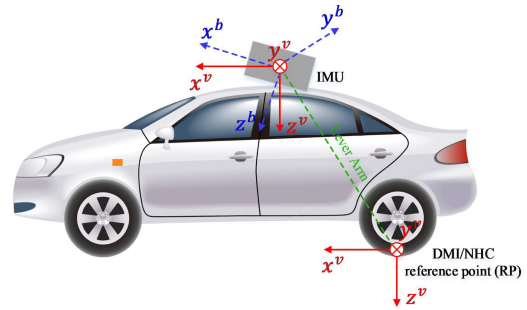


Fig. 1. Schematics of misalignment of the IMU frame with respect to the vehicle frame and of the lever arm between the IMU center and DMI/NHC reference point (RP).

geometry, satellite signal interference, or outages, especially in urban environments. The INS solution, especially based on the low-end inertial measurement unit (IMU), is affected by inertial sensor errors and diverges with time because of the integration process. Thus, it should be updated periodically using external measurements and/or vehicle dynamic constraints to restrain the navigation divergence [2].

Much research on multi-information fusion has been carried out using different auxiliary sensors to enhance the GNSS/INS integrated navigation accuracy under poor GNSS signals [3]. Due to the implementation simplicity and cost savings, the distance measurement instrument (DMI) and/or nonholonomic constraints (NHC) are the external auxiliary sensor and measurements commonly used in land vehicle navigation [4]. The DMI can provide the mileage traveled or the forward velocity in the vehicle frame. The NHC restricts the admissible direction of motion, e.g., a land vehicle cannot move in the directions perpendicular to the forward direction in the vehicle frame. The DMI in the form of the forward velocity and NHC can be used to develop 3-D velocity assistance to enhance the accuracy and reliability of land vehicle navigation in complex environments. However, two key mounting parameters exist representing the geometric relationship between the sensors when using auxiliary information from the DMI and/or NHC: First, the mounting angle reflects axes mismatch or misalignment between the IMU frame and the vehicle frame; second, the lever arm represents the spatial distance between the IMU center and the DMI reference point (RP), as shown in Fig. 1. Compensation for the mounting angle and lever arm is performed to realize frame unification and space unification, respectively. These two parameters need

to be considered and compensated when the DMI and NHC are exactly and reliably applied to GNSS/INS integration.

Here, we need to distinguish the lever arm between the IMU center and GNSS antenna, which can be estimated by an augmented navigation Kalman filter (KF) [5]. The required lever arm accuracy of the NHC for land vehicle navigation can be found in [6], and a simple estimation method for the NHC lever arm was proposed to further optimize the navigation solution. The DMI/NHC lever arm can also be estimated by a specific KF, but the estimation accuracy depends on the vehicle dynamics [7]. Although the lever arm can be measured using tape or the total stations in advance, the measurement accuracy may not be accurately guaranteed because of poor intervisibility and a complex vehicle structure. Hence, the lever arm between the IMU center and the valid point of the motion constraints must be estimated to better satisfy vehicle motion constraints. Generally, the mounting angle is difficult to measure accurately. Syed *et al.* [8] analyzed the required alignment of the inertial unit with respect to the vehicle by position drift errors during GNSS signal outages, but this accuracy level of angular misalignment cannot be applied to the high-accuracy navigation. Hong *et al.* [9] estimated the relative attitude between a GPS antenna array and an IMU, but this relative attitude is not the misalignment between the IMU frame and the vehicle frame. Hence, the misalignment of the IMU frame with respect to the vehicle frame needs to be estimated and compensated for accurately.

Some studies have been conducted on methods for estimating the mounting angle. According to the observations considered, the present methods can be divided into three categories: acceleration observations, velocity observations, and position observations. Vinande *et al.* [10] utilized the accelerometer output at rest on a horizontal road surface for pitch and roll angle estimation and a known forward acceleration on an assumed horizontal road surface to achieve yaw mounting angle estimation. Mu and Zhao [11] achieved misalignment estimation by using triaxial gyroscope and accelerometer measurements based on motion-mode recognition for micro electro mechanical system (MEMS) IMUs to be placed in an arbitrary arrangement. However, these acceleration-based estimation methods are affected by sensor errors (e.g., bias) or an acceleration (e.g., acceleration magnifies the coupling effect of mounting angles), and the misalignment estimation error is usually greater than 1° [10]. Wu *et al.* [7] designed a self-calibration algorithm using an adaptive extended KF based on velocity vector and height constraints and performed nonlinear observability to obtain a moderately sufficient condition for a successful calibration. Similar misalignment estimation methods based on the velocity vector observations can be found in [12] and [13], with some differences in the optimal filter and the constraints used. Different from the velocity-based estimation methods in the case of the DMI and NHC, the position-based method utilizes the position information obtained by the dead reckoning (DR) algorithm as the measurement of the optimal filter [14], [15]. Chen *et al.* [14] designed a DR scheme using the attitude, derived incremental distance measurements from GNSS/INS smoothing solutions, and integrated the derived with the GNSS/INS position to estimate the pitch and heading

mounting angles of the IMU. Wen *et al.* [15] constructed a position observation acquired by deducting the DR (odometer based) output position from the INS output position as the measurement for misalignment estimation. However, these methods utilize the KF as the optimal estimation method. Therefore, these methods strictly require prior knowledge on the accuracy of misalignment estimation and the measurement noise [16], [17].

Actually, misalignment estimation is the attitude identification between the IMU frame and the vehicle frame. The attitude estimation methods mainly include the KF, the quaternion algorithm, and parameter identification (e.g., least squares) [18]. The quaternion-based optimal estimation method can address those scenarios that have no prior initial attitude information available, and it is commonly used to solve the INS attitude initialization as an attitude optimization problem using multiple vector observations [19]–[21]. Therefore, we propose the quaternion-based misalignment estimation from velocity vector observations to address the shortcomings of the existing estimation methods. The main contributions of this article are as follows.

- 1) Using the quaternion-optimization-based estimation method can yield quick estimation speed (approximately 5 s). The utilization of the quaternion-based optimal estimation method eliminates the influence of prior knowledge, and it solves the problem of convergence caused by inaccurate initial information.
- 2) Velocity vector observations are used in the proposed mounting parameter estimation to ensure accuracy and reliability. The velocity-based estimation method has better accuracy than that using acceleration observations, and it directly acts on velocity-aided integrated navigation and does not require the high-accuracy position information.
- 3) Weighted recursive least squares (wRLS) are applied to estimate the lever arm considering the effect of velocity observation noise on the estimation accuracy, and it is helpful in determining the optimal valid location of holonomic constraints and realizing the full motion constraint potential.

The rest of this article is organized as follows. In Section II, the basic land vehicle velocity model is introduced. In Section III, the methods for estimating the mounting parameter, including mounting angle and lever arm, are described, and the error analysis is studied. In Section IV, the experimental results of the proposed misalignment method are presented and discussed to demonstrate its effectiveness and correctness. Finally, Section V concludes this article.

II. LAND VEHICLE VELOCITY MODEL

A. Land Vehicle Velocity Model

A rigorous model for the velocity in the vehicle frame (denoted by v -frame) is too complex to build directly since it requires more information, such as the steering angles, tire pressure, and slip angles. Hence, a simplified velocity model has been widely accepted in the application of land vehicle navigation. The NHC assumes that the land vehicle does not jump off the ground and does not slide along the ground; thus, these two velocity components of the vehicle in the plane perpendicular

to the forward direction (e.g., the x -axis) are zero. Hence, the lateral (y -axis) and vertical (z -axis) velocity measurements in the vehicle frame can be expressed as

$$\begin{cases} v_y^v = 0 \\ v_z^v = 0 \end{cases} \quad (1)$$

where v_y^v and v_z^v represent the velocity components of the vehicle in the plane perpendicular to the forward direction (x -axis). The superscript v represents the vehicle frame.

Ideally, the DMI measures the forward velocity of the DMI RP in the vehicle frame, as shown in Fig. 1. An uncalibrated DMI has a scale factor error, and the DMI output \tilde{v}_{dmi} satisfies

$$\tilde{v}_{\text{dmi}} = s_{\text{dmi}} \cdot v_f \quad (2)$$

where s_{dmi} is the DMI scale factor and v_f is the true forward velocity in the vehicle frame. The DMI in the form of the forward velocity and the NHC can be used to construct the 3-D velocity in the vehicle frame as follows:

$$\mathbf{v}_{\text{RP}}^v = \begin{bmatrix} v_x^v \\ v_y^v \\ v_z^v \end{bmatrix} = \begin{bmatrix} v_f \\ 0 \\ 0 \end{bmatrix} = \begin{bmatrix} \tilde{v}_{\text{dmi}}/s_{\text{dmi}} \\ 0 \\ 0 \end{bmatrix} \quad (3)$$

where \mathbf{v}_{RP}^v represents the velocity vector in the vehicle frame at the DMI/NHC RP, and v_x^v represents the forward velocity component of the vehicle velocity \mathbf{v}_{RP}^v .

B. Velocity Relationship Caused by Mounting Parameters

Owing to the existence of the lever arm, as shown in Fig. 1, the relationship between the velocity of the vehicle at the IMU center $\mathbf{v}_{\text{imu}}^n$ and that at the DMI/NHC RP \mathbf{v}_{RP}^n can be expressed in the following form based on the Coriolis theorem and the definition of the vehicle ground speed:

$$\mathbf{v}_{\text{RP}}^n = \mathbf{v}_{\text{imu}}^n + \mathbf{C}_b^n (\boldsymbol{\omega}_{eb}^b \times \mathbf{l}^b) \quad (4)$$

where \mathbf{C}_b^n is the direction cosine matrix (DCM), which represents the attitude matrix from the IMU frame to the navigation frame, $\boldsymbol{\omega}_{eb}^b$ represents the angular rate of the IMU frame relative to the earth frame in the IMU frame, and \mathbf{l}^b is the lever arm from the IMU center to the DMI RP in the IMU frame. In the absence of the DMI, the 3-D velocity can also be constructed from the velocity provided by the IMU as $v_f = |\mathbf{v}_{\text{imu}}^n + \mathbf{C}_b^n (\boldsymbol{\omega}_{eb}^b \times \mathbf{l}^b)|$.

The DMI and NHC are valid measurements in the vehicle frame; thus, using a DMI or an NHC as an aid requires considering the misalignment between the IMU frame and the vehicle frame. The velocity relationship can be further written as

$$\mathbf{v}_{\text{RP}}^v = \mathbf{C}_b^v [\mathbf{C}_n^b \mathbf{v}_{\text{imu}}^n + (\boldsymbol{\omega}_{eb}^b \times \mathbf{l}^b)] \quad (5)$$

where \mathbf{C}_n^b is the transpose matrix of \mathbf{C}_b^n and \mathbf{C}_b^v represents the attitude matrix from the IMU frame to the vehicle frame. \mathbf{C}_b^v can be written in terms of the misalignment angles as follows:

$$\mathbf{C}_b^v = \begin{bmatrix} c\theta c\varphi & c\theta s\varphi & -s\theta \\ -c\phi s\varphi + s\phi s\theta c\varphi & c\phi c\varphi + s\phi s\theta s\varphi & s\phi c\theta \\ s\phi s\varphi + c\phi s\theta c\varphi & -s\phi c\varphi + c\phi s\theta s\varphi & c\phi c\theta \end{bmatrix} \quad (6)$$

where c and s refer to the cosine and sine operators, respectively. ϕ , θ , and φ are the roll angle, pitch angle, and heading angle,

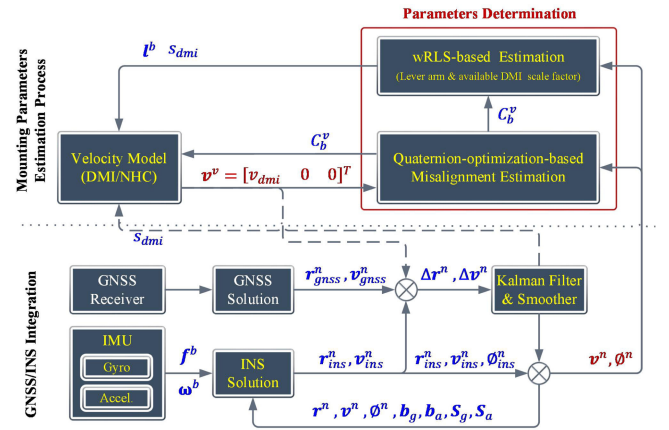


Fig. 2. Scheme block diagram of the mounting parameter (misalignment and lever arm) estimation for the velocity-aided GNSS/INS integration.

respectively; note that they are the mounting angles from the IMU frame to the vehicle frame.

III. MOUNTING PARAMETER ESTIMATION METHODS

In this section, a mounting parameter estimation scheme, including quaternion-based optimal misalignment estimation and lever arm estimation by the wRLS, is studied. The constructed velocity vector observations are derived from the velocity model and the GNSS/INS integrated solution. The smoothed integrated results are used to ensure the estimation accuracy of low-end systems. The specific block diagram of the mounting parameter estimation for velocity-aided GNSS/INS integration is shown in Fig. 2.

A. Quaternion-Based Optimal Attitude Determination

The attitude quaternion $\mathbf{q} = [q_s \ \mathbf{q}_v]^T$ is a four-parameter representation of a coordinate transformation matrix that is composed of a scalar part q_s and a 3-D vector part $\mathbf{q}_v = [q_1 \ q_2 \ q_3]^T$. The attitude quaternion satisfies the normalization constraint, which is

$$\mathbf{q}^T \mathbf{q} = 1 \quad (7)$$

where the superscript T denotes the transposition operator.

The relationship between the DCM and the corresponding quaternion vector is

$$\mathbf{C}(\mathbf{q}) = (q_s^2 - \mathbf{q}_v^T \mathbf{q}_v) \mathbf{I} + 2\mathbf{q}_v \mathbf{q}_v^T + 2q_s (\mathbf{q}_v \times) \quad (8)$$

where $\mathbf{C}(\mathbf{q})$ is the DCM corresponding to \mathbf{q} , \mathbf{I} is the identity matrix, and $(\mathbf{q}_v \times)$ is the skew-symmetric matrix.

The vector coordinate transformation formula expressed in quaternion form is

$$\boldsymbol{\alpha}(t) = \mathbf{q} \otimes \boldsymbol{\beta}(t) \otimes \mathbf{q}^* \quad (9)$$

where $\boldsymbol{\alpha}(t)$ and $\boldsymbol{\beta}(t)$ are two vector quaternions with zero scalar parts. t is the current time. \otimes denotes the quaternion product. The superscript $*$ represents the conjugate quaternion operator. Equation (9) can be transformed into a linear equation as in [17]

by right multiplying both sides by \mathbf{q}

$$\boldsymbol{\alpha}(t) \otimes \mathbf{q} - \mathbf{q} \otimes \boldsymbol{\beta}(t) = \mathbf{0}. \quad (10)$$

To obtain a linear equation in \mathbf{q} , the operator is defined as

$$[\mathbf{q}]^+ \triangleq \begin{bmatrix} q_s & -\mathbf{q}_v^T \\ \mathbf{q}_v & q_s \mathbf{I} + (\mathbf{q}_v \times) \end{bmatrix}, \quad [\mathbf{q}]^- \triangleq \begin{bmatrix} q_s & -\mathbf{q}_v^T \\ \mathbf{q}_v & q_s \mathbf{I} - (\mathbf{q}_v \times) \end{bmatrix}. \quad (11)$$

Quaternion multiplication satisfies the following relation:

$$\mathbf{q} \otimes \boldsymbol{\beta}(t) = [\mathbf{q}]^+ \boldsymbol{\beta}(t) = [\boldsymbol{\beta}(t)]^- \mathbf{q}. \quad (12)$$

Therefore, (12) can be rearranged as

$$\left([\boldsymbol{\alpha}(t)]^+ - [\boldsymbol{\beta}(t)]^- \right) \mathbf{q} = \mathbf{0}. \quad (13)$$

The optimal attitude quaternion \mathbf{q} can be taken as a minimization procedure [17], that is

$$\begin{aligned} \min_{\mathbf{q}} \int_0^{t_e} \left\| \left([\boldsymbol{\alpha}(t)]^+ - [\boldsymbol{\beta}(t)]^- \right) \mathbf{q} \right\|^2 dt \\ = \min_{\mathbf{q}} \mathbf{q}^T \int_0^{t_e} \left\| \left([\boldsymbol{\alpha}(t)]^+ - [\boldsymbol{\beta}(t)]^- \right) \right\|^2 dt \mathbf{q} \\ \triangleq \min_{\mathbf{q}} \mathbf{q}^T \mathbf{K} \mathbf{q}. \end{aligned} \quad (14)$$

Here, define

$$\mathbf{K} = \int_0^{t_e} \left\| \left([\boldsymbol{\alpha}(t)]^+ - [\boldsymbol{\beta}(t)]^- \right) \right\|^2 dt. \quad (15)$$

The constraint of (7) can be taken into account by the Lagrange multiplier method [22]; thus, the following gain function is defined as

$$g(\mathbf{q}) = \mathbf{q}^T \mathbf{K} \mathbf{q} - \lambda (\mathbf{q}^T \mathbf{q} - 1) \quad (16)$$

where λ is a real scalar that is chosen to satisfy the constraint. The quaternion optimization is transformed into the minimization of $g(\mathbf{q})$. Taking the derivative of the gain function $g(\mathbf{q})$ with respect to \mathbf{q} yields

$$\mathbf{K} \mathbf{q} = \lambda \mathbf{q}. \quad (17)$$

Equation (17) indicates that λ is an eigenvalue of \mathbf{K} . Substituting (17) into (16) yields

$$g(\mathbf{q}) = \lambda. \quad (18)$$

This equation indicates that λ is the minimum eigenvalue λ_{\min} of \mathbf{K} that can reach the minimum value of $g(\mathbf{q})$. Thus, the optimal attitude quaternion \mathbf{q}_{opt} is the eigenvector of \mathbf{K} with respect to the minimum eigenvalue. More clearly

$$\mathbf{K} \mathbf{q}_{\text{opt}} = \lambda_{\min} \mathbf{q}_{\text{opt}}. \quad (19)$$

B. Misalignment Angle Estimation

The misalignment angle estimation is the procedure of attitude identification between the IMU frame and the vehicle frame. The

basis of the quaternion-based optimization attitude estimation method is to construct the vectors $\boldsymbol{\alpha}(t)$ and $\boldsymbol{\beta}(t)$.

Here, set

$$\boldsymbol{\alpha}(t) = \mathbf{v}_{\text{RP}}^v(t) \quad (20)$$

$$\boldsymbol{\beta}(t) = \mathbf{C}_n^b(t) \mathbf{v}_{\text{imu}}^n(t) + (\boldsymbol{\omega}_{eb}^b(t) \times \mathbf{l}^b). \quad (21)$$

Equation (5) can be rewritten as

$$\boldsymbol{\alpha}(t) = \mathbf{C}_b^v \boldsymbol{\beta}(t). \quad (22)$$

Equation (22) can then be expressed in quaternion form as

$$\boldsymbol{\alpha}(t) = \mathbf{q}_b^v \otimes \boldsymbol{\beta}(t) \otimes \mathbf{q}_b^{v*} \quad (23)$$

where \mathbf{q}_b^v is the quaternion representation of misalignment angles from the IMU frame to the vehicle frame. The optimal \mathbf{q}_b^v can be obtained by (15) and (19) to complete the optimal estimation of the misalignment angle between the IMU frame and the vehicle frame. However, not all misalignment angles can be estimated based on the velocity observation.

Equation (5) can be transformed into the following equation by left multiplying both sides by \mathbf{C}_v^b :

$$\mathbf{C}_v^b \mathbf{v}_{\text{RP}}^v = \mathbf{C}_n^b \mathbf{v}_{\text{imu}}^n + (\boldsymbol{\omega}_{eb}^b \times \mathbf{l}^b). \quad (24)$$

Substituting (6) into (24) yields

$$(\mathbf{C}_v^b)^T \begin{bmatrix} v_f \\ 0 \\ 0 \end{bmatrix} = v_f \begin{bmatrix} c\theta c\varphi \\ c\theta s\varphi \\ -s\theta \end{bmatrix} = \mathbf{C}_n^b \mathbf{v}_{\text{imu}}^n + (\boldsymbol{\omega}_{eb}^b \times \mathbf{l}^b). \quad (25)$$

The above equation indicates that the velocity observation is irrelevant to the misalignment angle ϕ (along the forward axis), that is, ϕ cannot be estimated.

If the vehicle is running along a straight line with time-varying velocity, which means that $\boldsymbol{\omega}_{eb}^b = \mathbf{0}$ and $v_f \neq 0$, then (25) can be rewritten as

$$\mathbf{C}_v^b \mathbf{v}_{\text{RP}}^v = \mathbf{C}_n^b \mathbf{v}_{\text{imu}}^n. \quad (26)$$

This equation indicates that the misalignment estimation is not affected by the lever arm under the condition of running along a straight line. This sufficient condition can be used to distinguish the estimation of misalignment and the lever arm and reduce the interaction between the two mounting parameters.

C. wRLS-Based Lever Arm Estimation

Usually, the lever arm can be accurately measured using tape or the total station in advance, but some measurement error exists due to poor visibility conditions. Hence, the lever arm can be estimated based on the initial values to further increase the accuracy. Equation (5) can be rearranged as follows:

$$(\boldsymbol{\omega}_{eb}^v \times) \mathbf{l}^v = \mathbf{v}_{\text{RP}}^v - \mathbf{C}_b^v \mathbf{C}_n^b \mathbf{v}_{\text{imu}}^n. \quad (27)$$

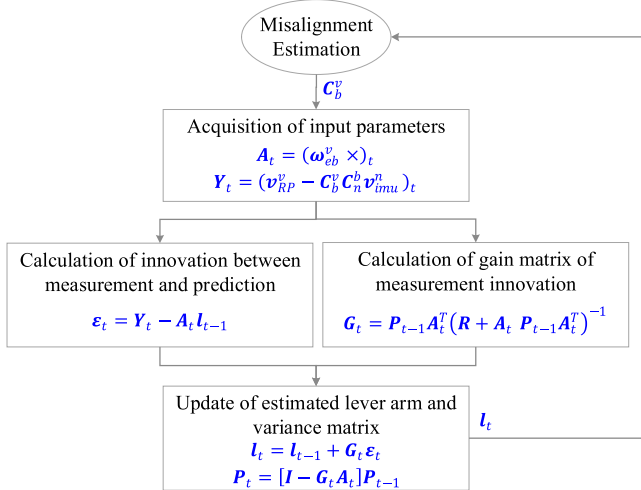


Fig. 3. Procedure of wRLS-based lever arm estimation.

This is a typical least squares estimation. To reduce the resource and memory consumption of the least squares method, the wRLS algorithm, which eliminates the inversion operation, is utilized to estimate the lever arm and the scale factor. The specific estimation procedure based on the wRLS is shown in Fig. 3.

To further study the estimation effect of the lever arm in the vehicle frame, (27) can be converted to a representation in the vehicle frame, and it can be written in the following form:

$$\begin{bmatrix} v_x^v \\ v_y^v \\ v_z^v \end{bmatrix} = \begin{bmatrix} v_{imu,x}^v \\ v_{imu,y}^v \\ v_{imu,z}^v \end{bmatrix} + \begin{bmatrix} 0 & -\omega_{eb,z}^v & \omega_{eb,y}^v \\ \omega_{eb,z}^v & 0 & -\omega_{eb,x}^v \\ -\omega_{eb,y}^v & \omega_{eb,x}^v & 0 \end{bmatrix} \begin{bmatrix} l_x^v \\ l_y^v \\ l_z^v \end{bmatrix} \quad (28)$$

where $v_{imu,x}^v$, $v_{imu,y}^v$, and $v_{imu,z}^v$ represent the three components of IMU velocity in the vehicle frame; $\omega_{eb,x}^v$, $\omega_{eb,y}^v$, and $\omega_{eb,z}^v$ represent the three components of the angular rate of the IMU frame relative to the earth frame in the vehicle frame; and l_x^v , l_y^v , and l_z^v are the three components of the lever arm from the IMU center to the valid point for the NHC in the vehicle frame.

For land vehicles, significant angular motion around the vertical axis (i.e., z component) due to turning will occur, while a relatively small angular rate around the longitudinal and lateral axes (i.e., x and y components), that is, $\omega_{eb,x}^v \approx 0$ and $\omega_{eb,y}^v \approx 0$, will be observable. Hence, (28) can be reduced to

$$v_x^v = v_{imu,x}^v - \omega_{eb,z}^v l_y^v, \quad v_y^v = v_{imu,y}^v + \omega_{eb,z}^v l_x^v. \quad (29)$$

This indicates that the longitudinal and lateral components of the lever arm are easy to estimate during turning for land vehicle applications. If the forward velocity provided by the DMI is not available, only the longitudinal lever arm can be estimated based on the second equation of (29).

D. Influence Factor of Misalignment Estimation Accuracy

The perturbation method was utilized to analyze the influence of the velocity error and attitude error on the misalignment error. Neglecting the effect of the second-order small quantity, (26) can be rearranged as (details of the derivation can be found in the



Fig. 4. Trajectory of the land vehicle test (marked by the red dotted line, from Google Earth).

Appendix)

$$-v_{RP}^v \times \delta\phi_{\text{mis}} = C_b^v C_n^b (\delta v_{imu}^n - v_{imu}^n \times \delta\phi) \quad (30)$$

where $\delta\phi_{\text{mis}}$ represents the misalignment angle error, with $\delta\phi_{\text{mis}} = [\delta\phi \ \delta\theta \ \delta\varphi]^T$. Considering (3), (30) can be converted to the vehicle frame as

$$\begin{bmatrix} 0 \\ \delta\varphi \\ -\delta\theta \end{bmatrix} = C_b^v C_n^b \left(\frac{\delta v_{imu}^n}{v_f} - \frac{1}{v_f} \begin{bmatrix} -v_D^n \delta\phi_y + v_E^n \delta\phi_z \\ v_D^n \delta\phi_x - v_N^n \delta\phi_z \\ -v_E^n \delta\phi_x + v_N^n \delta\phi_y \end{bmatrix} \right) \quad (31)$$

where v_N^n , v_E^n , and v_D^n represent the north, east, and down velocities in the navigation frame, respectively. $\delta\phi_x$, $\delta\phi_y$, and $\delta\phi_z$ represent the roll angle error, pitch angle error, and heading angle error of the GNSS/INS integrated navigation results, respectively.

Equation (31) indicates that the influence of velocity error can be reduced by increasing the forward speed. However, the effect of velocity error can be taken out of consideration because it can be generally controlled within centimeter per second (cm/s) in the presence of GNSS auxiliary information. Additionally, the heading misalignment angle is affected mainly by the roll and heading errors, while the pitch misalignment angle is affected by the roll and pitch errors. For the low-end IMU, the heading error is the main influential factor because the heading error is larger than the horizontal attitude error and the horizontal velocity is greater than the vertical velocity for land vehicular applications.

IV. TEST RESULTS AND DISCUSSION

A. Land Vehicle Test Description

The land vehicle test was conducted in an open-sky area in Wuhan on December 10, 2019; the trajectory is shown in Fig. 4. The red trajectory line indicates that the GNSS signal observation was in good condition, and the number of visible GNSS satellites was always greater than 6 during the test to ensure the estimation accuracy of the mounting parameter because

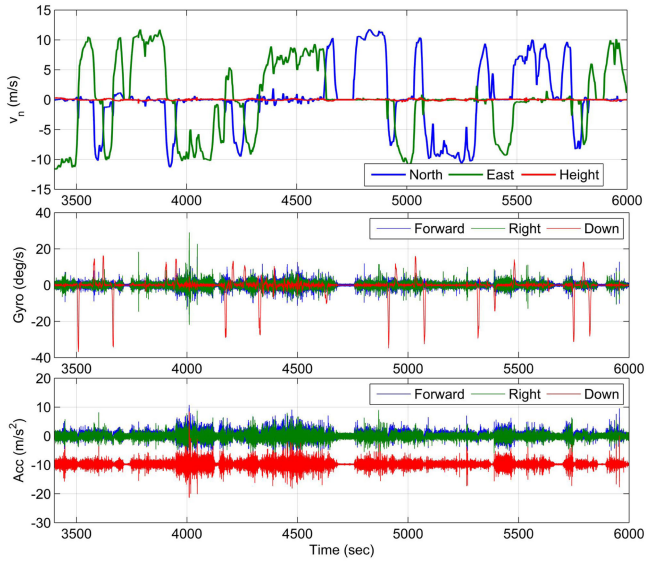


Fig. 5. Land vehicle velocity (top) in the navigation frame, and the angular rate (middle) and the specific force (bottom) in the IMU frame.

TABLE I
SPECIFICATIONS OF DIFFERENT-GRADE IMUS

Sensor	Main Error Sources	IMU 1	IMU 2	IMU 3
		Navigation (Leader A15)	MEMS IMU	
			Industrial (ADIS16465)	Consumer (ASM330LHH)
Gyro	bias instability (°/h)	0.03	48	27
	white noise (°/√h)	0.003	0.1	0.63
Accel.	bias instability (mGal)	15	50	300
	white noise (m/s/√h)	0.03	0.1	0.35

the navigation error will drift without GNSS information assistance, resulting in the inability to perform mounting parameter estimation.

Fig. 5 shows the land vehicle velocity in the navigation frame and the angular rate and acceleration in the IMU frame. The operation speed limits the range between 20 and 50 km/h, and frequent U-turns and turns (angular rate is less than 40°/s) occur to ensure sufficient movement; the running acceleration is basically controlled at 2 m/s². The road is relatively flat without significant slopes, and some instantaneous accelerations (e.g., approximately 10 m/s²) and horizontal angular rates (e.g., approximately 20°/s) occur due to the vibration of vehicles caused by rough roads or bumps.

In addition, a land vehicle test with different-grade IMUs was carried out to validate the feasibility of the proposed mounting parameter estimation scheme and analyze the main error source that influences the accuracy of misalignment estimation. Three integrated systems, including one navigation-grade IMU and two different MEMS IMUs, were used to investigate the performance of mounting parameters using the proposed method, and their specifications of the three IMUs are listed in Table I. The two low-end MEMS IMUs were used to analyze the main factors influencing parameter estimation and to study the estimation capability of the proposed method for low-end systems.

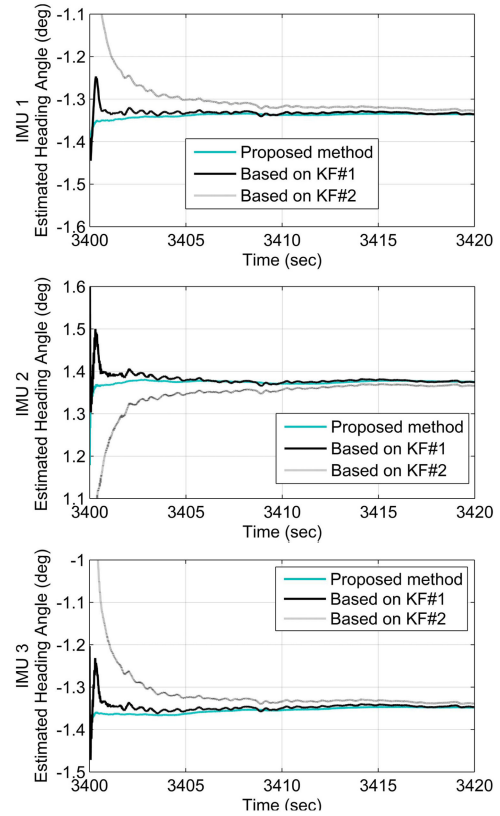


Fig. 6. Comparison of the heading mounting angles of different estimation methods, including the quaternion-based method and KF-based method.

B. Comparison of the Mounting Angle Estimation Under Different Methods

The acceleration-based estimation methods are affected by the performance of the MEMS IMU, and the misalignment estimation accuracy is usually greater than 0.1°. An initial convergence problem occurs in the KF-based estimation method (denoted as the KF-based method). To verify the mounting angle estimation speed and stability using the quaternion-based optimal attitude determination method, we mainly compared the estimated mounting angle with that of the estimation method based on KF.

Here, the heading mounting angle is taken as an example because the pitch angle has similar behavior. Two initialization settings were designed in the KF-based method: KF#1 indicates that the KF-based method applied reasonable initial statistical values (e.g., the initial heading accuracy is set at 10°), while KF#2 indicates the KF-based method with unreasonable values (e.g., the initial heading accuracy is set at 0.1°).

Fig. 6 shows the heading mounting angle estimated by the different estimation methods. Note that the three systems have their own mounting angles; thus, the difference in the estimated values is not related to a difference in accuracy. Fig. 6 reveals an obvious convergence of the heading mounting angle for the KF-based estimation method. KF#1 requires 10 s to reach stability at 0.01°, while KF#2 does not converge within 20 s. By contrast,

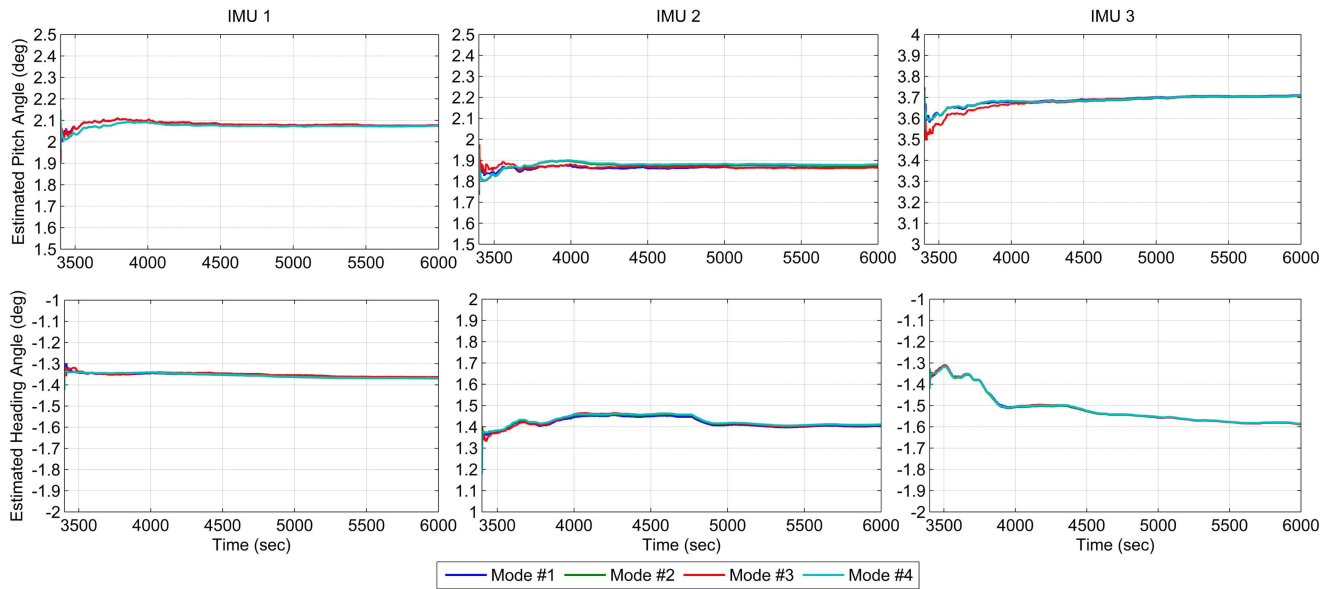


Fig. 7. Estimated mounting angles by the quaternion-based optimal attitude determination method under different modes for land vehicles.

TABLE II
LIST OF DIFFERENT ESTIMATION CONFIGURATIONS

Mode Type	With DMI	To estimate lever arm*	To estimate DMI scale factor
Mode #1	yes	yes	yes
Mode #2	no	yes	no
Mode #3	yes	no	yes
Mode #4	no	no	no

* For lever arm, "no" represents the utilization of a measured lever arm using tape.

the heading mounting angle estimated by the proposed method can quickly converge under the same conditions with the time required to reach stability at 0.01° being less than 5 s.

C. Mounting Parameter Estimation in Different Modes

Considering the availability of the DMI and the necessity of estimating the lever arm and DMI scale factor, Table II lists the different estimation configurations of data analysis in this article. Note that Mode #2 and Mode #4 utilize the constructed forward velocity to carry out the estimation of mounting parameters; thus, Mode #2 provides only the estimated longitudinal lever arm in the vehicle frame.

Fig. 7 shows the estimated mounting angles under different modes over a period of time (approximately 0.72 h). The results show that the estimation of the mounting angle can quickly converge (less than 20 s), but the performance is ranked as IMU1, IMU2, and IMU3 from high to low in terms of the stability of the estimated results. As given in Table III, the estimated pitch angle fluctuation intensity of the three IMUs is approximately 0.02° ; the estimated heading angle fluctuation intensities of IMU1 and IMU2 are, respectively, approximately 0.01° and 0.02° , while that of IMU3 is greater than 0.07° . These results are in exact

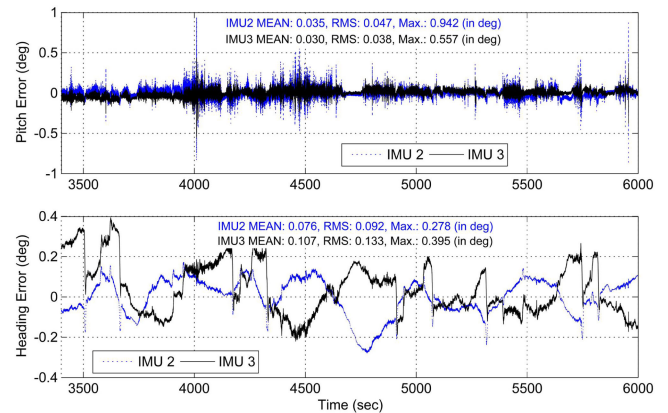


Fig. 8. Attitude error (with statistical values) of MEMS-based integrated systems, including the pitch error (top) and the heading error (below).

accordance with (31), which can be used to calculate the heading mounting angle estimation accuracy; that is, the heading error of the integrated system is the main factor influencing the heading mounting angle. As shown in Fig. 8, the heading accuracy of IMU3 is worse, especially at the beginning.

For the different modes, as shown in Fig. 7 and Table III, the difference in estimated values is basically less than 0.01° , which is quite small. This result indicates that the estimation of the mounting angle can be completed without the DMI on the basis of ensuring the same accuracy level. The lever arm, especially the longitudinal lever arm, needs to be estimated during turning to ensure the estimation performance of the mounting angle because Mode #2 estimates only the longitudinal lever arm and provides a reasonable mounting angle estimation. In addition, due to the vibration caused by unstable installation, the pitch

TABLE III
STATISTICS OF ESTIMATED MOUNTING ANGLES UNDER DIFFERENT MODES FOR LAND VEHICLES

Mode	Statistics	Statistical Values of Estimated Mounting Angles of Three IMUs					
		IMU 1		IMU 2		IMU 3	
		Pitch (°)	Heading (°)	Pitch (°)	Heading (°)	Pitch (°)	Heading (°)
Mode #1	MEAN	2.082	-1.356	1.863	1.419	3.687	-1.515
	STD	0.012	0.010	0.007	0.024	0.024	0.074
Mode #2	MEAN	2.073	-1.356	1.874	1.424	3.684	-1.516
	STD	0.012	0.010	0.014	0.024	0.023	0.073
Mode #3	MEAN	2.082	-1.351	1.868	1.424	3.678	-1.514
	STD	0.013	0.010	0.007	0.029	0.037	0.075
Mode #4	MEAN	2.073	-1.355	1.879	1.428	3.686	-1.514
	STD	0.012	0.010	0.015	0.024	0.023	0.073

Note: MEAN represents the mean value of the data series; STD is the abbreviation for standard deviation.

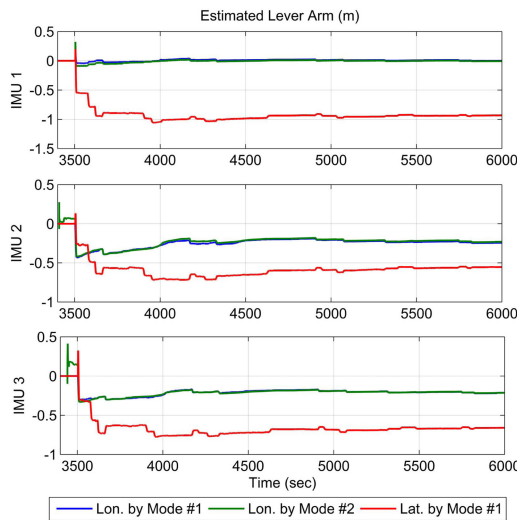


Fig. 9. Estimated longitudinal (Lon.) and lateral (Lat.) lever arm in the vehicle frame based on the wRLS method under different modes.

error of IMU2 slightly larger than that of IMU3, as shown in Fig. 8, so the estimation repeatability of the IMU2 pitch mounting angle is slightly larger than 0.01°, which is worse than that of IMU3.

Fig. 9 shows the estimated longitudinal and lateral lever arms based on the wRLS under different modes. Mode #2 provides only the longitudinal lever arm estimation in the absence of the DMI by using the NHC information. The estimation of the lever arm depends on the angular rate around the vertical axis (z -axis); thus, the corresponding estimated values fluctuate during U-turns and other turns. The estimated accuracies of the longitudinal lever arm achieved by Mode #1 and Mode #2 are basically the same. For IMU2, the estimation stability of the lever arm is worse because of the obvious angular velocity vibration around the lateral axis (y -axis) due to the unstable installation; this issue also affects the estimation of the pitch mounting angle of IMU2, as shown in Fig. 8. Notably, the estimated lever arm values of IMU2 and IMU3 are close because they are installed close to each other.

Table IV lists the comparison between the estimated lever arm and the measured lever arm by tape and the corresponding statistical lateral velocity. Clearly, an error of approximately

TABLE IV
COMPARISON OF THE DMI/NHC LEVER ARMS BY DIFFERENT METHODS

Sensors	Methods	Parameters in the Vehicle Frame		
		DMI/NHC Lever Arm (m)		Statistical Lateral Velocity (m/s)
		Longitudinal	Lateral	
IMU 1	Estimated	-0.005	-0.932	0.022
	Measured	-0.205	-1.081	0.042
IMU 2	Estimated	-0.243	-0.556	0.040
	Measured	-0.667	-0.684	0.050
IMU 3	Estimated	-0.213	-0.660	0.024
	Measured	-0.499	-0.787	0.046

0.2 m between the estimated lever arm and the measured lever arm exists, except for the longitudinal distance of IMU2. The correctness of mounting parameter estimation can be validated by checking the lateral and vertical velocities in the vehicle frame because no significant velocity component should exist in these two directions to satisfy the NHC. Considering that the lateral velocity in the vehicle frame is more seriously and obviously affected by the mounting parameter during U-turns and other turns, a statistical analysis of the lateral velocity in the vehicle frame during U-turns and other turns was conducted. Clearly, the statistical lateral velocity based on the estimated lever arm is better than that based on the measured lever arm, with the corresponding root-mean-square (RMS) being approximately 0.02 m/s.

The results of the land vehicle test show that the proposed mounting parameter estimation scheme is effective and correct by the statistical lateral velocity in the vehicle frame and that the heading error of integrated systems is the main factor impacting the mounting parameter estimation accuracy. Moreover, the estimation of the mounting angle and longitudinal lever arm can be completed without the DMI under the same accuracy level.

D. Agricultural Tractor Test

An agricultural tractor test was conducted in an open-sky area in Wuhan on February 15, 2017, and a low-end integrated system based on the MEMS IMU (ADIS16460, its navigation performance is comparable with IMU3, as given in Table I) was used to evaluate the performance of mounting parameter estimation. A dual-antenna GNSS heading was applied to enhance the integrated heading accuracy and further compare the influence

TABLE V
SPECIFICATIONS OF LOW-END INTEGRATED SYSTEM BASED ON MEMS IMU

Sensors		Main Error Performance	
MEMS IMU (ADIS16460)	Gyro	bias instability ($^{\circ}/h$, 1σ)	12
		white noise ($^{\circ}/\sqrt{h}$)	0.2
	Accel.	bias instability (mGal, 1σ)	100
		white noise (m/s/ \sqrt{h})	0.2
GNSS	Heading (degree) on 2 m baseline (RMS) : 0.08°		

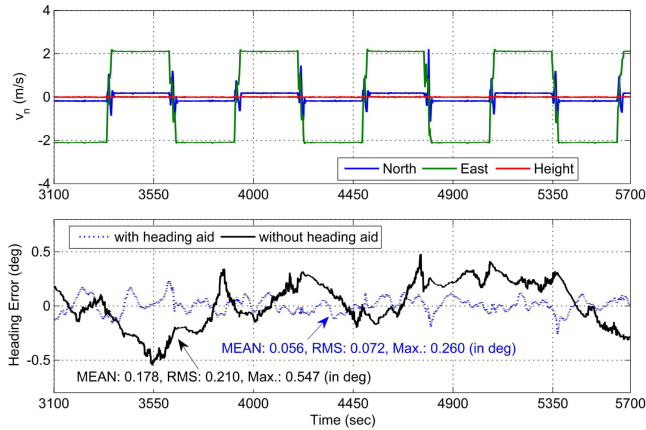


Fig. 10. Tractor velocity (top) and the heading error (bottom) with/without GNSS heading aid of the low-end system in the navigation frame.

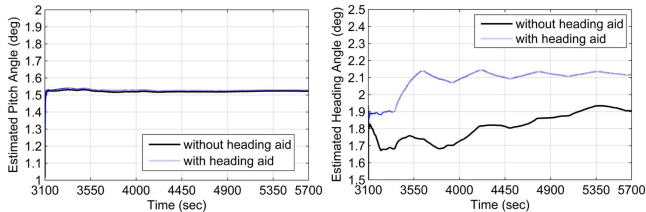


Fig. 11. Mounting angles estimated by the quaternion-based optimal attitude determination method with/without heading aid for the agricultural tractor.

of the heading error on the estimation accuracy. **Table V** lists the specifications of this low-end integrated system.

Fig. 10 shows the agricultural tractor velocity and the heading error of the low-end integrated system in the navigation frame. Here, the operating speed is approximately 2.0 m/s, and eight U-turns are required for sufficient movement. The heading error, which is controlled within approximately 0.5° , is obtained by calculating the difference from the dual-antenna GNSS heading with an accuracy of approximately 0.07° based on a 1.5 m baseline. **Fig. 11** shows the mounting angles estimated by the quaternion-based optimal attitude determination method with/without heading aid for the agricultural tractor. For the estimated pitch angles, the blue line and the black line basically overlap. The results show that the fluctuation of the estimated pitch mounting angle is obviously less than 0.01° , and it is not affected by the integrated heading error; the fluctuation of the estimated heading mounting angle is approximately 0.2° , and

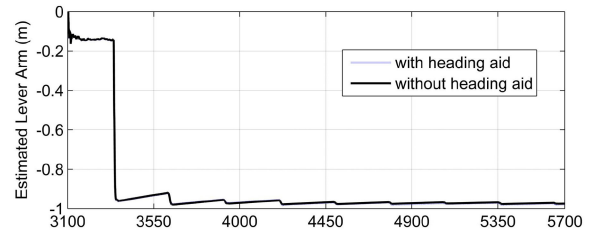


Fig. 12. Estimated longitudinal (Lon.) lever arm in the vehicle frame based on the wRLS method with/without heading aid.

it is significantly affected by the integrated heading error. This outcome further proves that the heading error of the integrated system is the main factor influencing the heading mounting angle, and that it has little effect on the pitch mounting angle estimation.

Fig. 12 shows the estimated longitudinal lever arm based on the wRLS under different modes. Clearly, the blue and the black lines overlap, frequent U-turns can accelerate the convergence of longitudinal lever arm estimation, and the integrated heading error has less influence on the lever arm estimation.

V. CONCLUSION

Precise determination of the mounting parameter is necessary to ensure the navigation accuracy of multi-information fusion, especially for the velocity model, which is used as necessary auxiliary information in land vehicle navigation. In this article, we proposed an optimal estimation scheme based on the velocity vector observations to estimate the mounting parameter. The quaternion-based optimal attitude determination method was used to estimate the mounting angle, and the wRLS was applied to estimate the lever arm. The perturbation method was utilized to analyze the influence of the velocity error and attitude error on the misalignment error.

A land vehicle test and an agricultural tractor test were carried out to verify the feasibility and correctness of the proposed estimation scheme under different dynamic conditions. In particular, low-end integrated systems based on MEMS IMU were utilized to analyze the main factor influencing the estimation accuracy. The results show that the mounting parameters estimated by the proposed method can better satisfy vehicle motion constraints, and that the statistical lateral velocity was better than 0.03 m/s. Moreover, the integrated heading error, which had little effect on other parameter estimations, was the main factor influencing the estimated heading misalignment accuracy.

The proposed estimation scheme can be further applied to multisensor mounting parameter estimation from velocity vector observations, especially for low-end systems under high-precision navigation requirements.

APPENDIX

The influence of the navigation error on the misalignment estimation accuracy is derived in detail as follows. Without considering the influence of the lever arm, (28) can be rewritten

as

$$\left(\hat{C}_b^v\right)^T \hat{\mathbf{v}}_{\text{RP}}^v = \hat{C}_b^v \hat{\mathbf{v}}_{\text{imu}}^n \quad (32)$$

where the operator $\hat{\cdot}$ denotes the estimated or computed values. The perturbation of the velocity and attitude matrix can be expressed as

$$\begin{aligned} \hat{C}_b^v &= (I - \delta\phi_{\text{mis}} \times) C_b^v \\ \hat{C}_b^n &= (I - \delta\phi \times) C_b^n \\ \hat{\mathbf{v}}_{\text{imu}}^n &= \mathbf{v}_{\text{imu}}^n + \delta\mathbf{v}_{\text{imu}}^n \end{aligned} \quad (33)$$

where the operator δ denotes the errors. Hence, the error perturbation analysis of (32) can be obtained as follows:

$$\begin{aligned} &((I - \delta\phi_{\text{mis}} \times) C_b^v)^T \mathbf{v}_{\text{RP}}^v \\ &= ((I - \delta\phi \times) C_b^n)^T (\mathbf{v}_{\text{imu}}^n + \delta\mathbf{v}_{\text{imu}}^n). \end{aligned} \quad (34)$$

Developing the perturbation equation and neglecting the effect of the second-order small quantity yield

$$-(C_b^v)^T (\mathbf{v}_{\text{RP}}^v \times) \delta\phi_{\text{mis}} = (C_b^n)^T \delta\mathbf{v}_{\text{imu}}^n - (C_b^n)^T (\mathbf{v}_{\text{imu}}^n \times) \delta\phi. \quad (35)$$

Considering (6), (35) can be converted to the vehicle frame as

$$\begin{aligned} &\begin{bmatrix} 0 & 0 & 0 \\ 0 & 0 & v_f \\ 0 & -v_f & 0 \end{bmatrix} \begin{bmatrix} \delta\phi \\ \delta\theta \\ \delta\varphi \end{bmatrix} \\ &= C_b^v (C_b^n)^T \left(\delta\mathbf{v}_{\text{imu}}^n - \begin{bmatrix} 0 & -v_D^n & v_E^n \\ v_D^n & 0 & -v_N^n \\ -v_E^n & v_N^n & 0 \end{bmatrix} \begin{bmatrix} \delta\phi_x \\ \delta\phi_y \\ \delta\phi_z \end{bmatrix} \right). \end{aligned} \quad (36)$$

Then, the following form can be obtained:

$$\begin{bmatrix} 0 \\ \delta\varphi \\ -\delta\theta \end{bmatrix} = C_b^v C_b^n \left(\frac{\delta\mathbf{v}_{\text{imu}}^n}{v_f} - \frac{1}{v_f} \begin{bmatrix} -v_D^n \delta\phi_y + v_E^n \delta\phi_z \\ v_D^n \delta\phi_x - v_N^n \delta\phi_z \\ -v_E^n \delta\phi_x + v_N^n \delta\phi_y \end{bmatrix} \right). \quad (37)$$

ACKNOWLEDGMENT

The authors would like to thank Wuhan MAP Space Time Navigation Technology, Inc., and Wuxi Kalman Navigation, Inc., for their platform support in the data collection process.

REFERENCES

- [1] Y. Kim, J. An, and J. Lee, "Robust navigational system for a transporter using GPS/INS fusion," *IEEE Trans. Ind. Electron.*, vol. 65, no. 4, pp. 3346–3354, Apr. 2018.
- [2] B. Wang, Q. Ren, Z. Deng, and M. Fu, "A self-calibration method for nonorthogonal angles between gimbals of rotational inertial navigation system," *IEEE Trans. Ind. Electron.*, vol. 62, no. 4, pp. 2353–2362, Apr. 2015.
- [3] X. Li, W. Chen, C. Chan, B. Li, and X. Song, "Multi-sensor fusion methodology for enhanced land vehicle positioning," *Inf. Fusion*, vol. 46, pp. 51–62, 2019.
- [4] M. Klomp, M. Jonasson, L. Laine, L. Henderson, E. Regolin, and S. Schumi, "Trends in vehicle motion control for automated driving on public roads," *Veh. Syst. Dyn.*, vol. 57, no. 7, pp. 1028–1061, 2019.

- [5] A. Borko, I. Klein, and G. Even-Tzur, "GNSS/INS fusion with virtual lever-arm measurements," *Sensors*, vol. 18, no. 7, 2018, Art. no. 2228.
- [6] Q. Zhang, Y. Hu, and X. Niu, "Required lever arm accuracy of non-holonomic constraint for land vehicle navigation," *IEEE Trans. Veh. Technol.*, vol. 69, no. 8, pp. 8305–8316, Aug. 2020.
- [7] Y. Wu, C. Goodall, and N. El-Sheimy, "Self-calibration for IMU/odometer land navigation: Simulation and test results," in *Proc. Int. Tech. Meeting Inst. Navig.*, San Diego, CA, USA, 2010, pp. 839–849.
- [8] Z. F. Syed, P. Aggarwal, X. Niu, and N. El-Sheimy, "Civilian vehicle navigation: Required alignment of the inertial sensors for acceptable navigation accuracies," *IEEE Trans. Veh. Technol.*, vol. 57, no. 6, pp. 3402–3412, Nov. 2008.
- [9] S. Hong, M. H. Lee, S. H. Kwon, and H. H. Chun, "A car test for the estimation of GPS/INS alignment errors," *IEEE Trans. Intell. Transp. Syst.*, vol. 5, no. 3, pp. 208–218, Sep. 2004.
- [10] E. Vinande, P. Axelrad, and D. Akos, "Mounting-angle estimation for personal navigation devices," *IEEE Trans. Veh. Technol.*, vol. 59, no. 3, pp. 1129–1138, Mar. 2010.
- [11] M. Mu and L. Zhao, "A GNSS/INS-integrated system for an arbitrarily mounted land vehicle navigation device," *GPS Solutions*, vol. 23, no. 4, 2019, Art. no. 112.
- [12] L. Li *et al.*, "Online calibration and compensation of total odometer error in an integrated system," *Measurement*, vol. 123, pp. 69–79, 2018.
- [13] Z. Liu, N. El-Sheimy, and Y. Qin, "Low-cost INS/odometer integration and sensor-to-sensor calibration for land vehicle applications," in *Proc. IAG/CPGPS Int. Conf. GNSS+ (ICG + 2016)*, Shanghai, China, 2016, pp. 1–2.
- [14] Q. Chen, Q. Zhang, and X. Niu, "Estimate the pitch and heading mounting angles of the IMU for land vehicular GNSS/INS integrated system," *IEEE Trans. Intell. Transp. Syst.*, pp. 1–13, May. 2020.
- [15] Z. Wen, G. Yang, Q. Cai, and Y. Sun, "Odometer aided SINS in-motion alignment method based on backtracking scheme for large misalignment angles," *IEEE Access*, vol. 8, pp. 7937–7948, 2019.
- [16] K. Taizhong, F. Jiancheng, and W. Wei, "Quaternion-optimization-based in-flight alignment approach for airborne POS," *IEEE Trans. Instrum. Meas.*, vol. 61, no. 11, pp. 2916–2923, Nov. 2012.
- [17] M. Wu, Y. Wu, X. Hu, and D. Hu, "Optimization-based alignment for inertial navigation systems: Theory and algorithm," *Aerosp. Sci. Technol.*, vol. 15, no. 1, pp. 1–17, 2011.
- [18] B. Liu, S. Wei, J. Lu, J. Wang, and G. Su, "Fast self-alignment technology for hybrid inertial navigation systems based on a new two-position analytic method," *IEEE Trans. Ind. Electron.*, vol. 67, no. 4, pp. 3226–3235, Apr. 2020.
- [19] L. Chang, Y. Li, and B. Xue, "Initial alignment for a doppler velocity log-aided strapdown inertial navigation system with limited information," *IEEE/ASME Trans. Mechatronics*, vol. 22, no. 1, pp. 329–338, Feb. 2017.
- [20] Y. Huang, Y. Zhang, and X. Wang, "Kalman-filtering-based in-motion coarse alignment for odometer-aided SINS," *IEEE Trans. Instrum. Meas.*, vol. 66, no. 12, pp. 3364–3377, Dec. 2017.
- [21] Y. Wu, J. Wang, and D. Hu, "A new technique for INS/GNSS attitude and parameter estimation using online optimization," *IEEE Trans. Signal Process.*, vol. 62, no. 10, pp. 2642–2655, May 2014.
- [22] M. D. Shuster and S. D. Oh, "Three-axis attitude determination from vector observations," *J. Guid. Control*, vol. 4, no. 1, pp. 70–77, 1981.



Quan Zhang received the B.S. degree in geomatics engineering from the Shandong University of Science and Technology, Qingdao, China, in 2009, and the Ph.D. degree in geodesy and survey engineering from Wuhan University, Wuhan, China, in 2015.

From 2017 to 2018, he was a Postdoctoral Researcher with the Digital Photogrammetry Research Group, Lyles School of Civil Engineering, Purdue University. He is currently an Associate Research Fellow with Global Navigation Satellite System (GNSS) Research Center, Wuhan University. His research interests include inertial navigation and GNSS/inertial navigation system integration technology.



Yuanqian Hu received the B.Eng. degree in navigation engineering from Wuhan University, Wuhan, China, in 2017, and the M.Eng. degree in navigation, guidance, and control from Global Navigation Satellite System (GNSS) Research Center, Wuhan University, in 2020.

He is currently with Qianxun Spatial Intelligence, Inc, Shanghai, China. His research direction focuses on GNSS/inertial navigation system integration and its simulation.



Tisheng Zhang received the B.Sc. and Ph.D. degrees in communication and information systems from Wuhan University, Wuhan, China, in 2008 and 2013, respectively.

He is an Associate Professor with Global Navigation Satellite System (GNSS) Research Center, Wuhan University. His research interest focuses on the fields of GNSS receiver and multi-sensor deep integration.



Shanshan Li received the B.S. degree from the School of Geodesy and Geomatics, Wuhan University, Wuhan, China, in 2015, and the M.S. degree from Global Navigation Satellite System Research Center, Wuhan University, in 2018, both in geomatics engineering.

She is currently with Qianxun Spatial Intelligence, Inc, Shanghai, China. Her current research interest focuses on information fusion and its applications, such as inertial navigation and integrated navigation.



Xiaoji Niu received the B.Eng.(Hons.) degree in mechanical and electrical engineering and the Ph.D. degree from Tsinghua University, Beijing, China, in 1997 and 2002, respectively.

From 2003 to 2007, he was a Postdoctoral Fellow with Mobile Multisensor Systems Research Group, Department of Geomatics Engineering, University of Calgary, and from 2007 to 2009, a Senior Scientist with SiRF Technology, Inc. He is currently a Professor with Global Navigation Satellite System (GNSS) Research Center, Wuhan University, Wuhan, China. His research interests include an inertial navigation system (INS) and GNSS/INS integration.